JPPIPA 11(12) (2025)

Jurnal Penelitian Pendidikan IPA

http://jppipa.unram.ac.id/index.php/jppipa/index

Spatio-Temporal Analysis of Land Cover for Estimating UHI Using GEE in Gorontalo City

La Ode Juni Akbar[1,3*], Arthur Gani Koto[2], Ahmad Syamsu Rijal[2]

[1] Student in Geography Study Program, University Muhammadiyah Gorontalo, Gorontalo, Indonesia.
[2] Geography Study Program, Universitas Muhammadiyah Gorontalo, Gorontalo, Indonesia.
[3] Regional Planing Study Program, University Bina Taruna Gorontalo, Gorontalo, Indonesia

Received: October 30, 2025
Revised: December 11, 2025
Accepted: December 25, 2025
Published: December 31, 2025

Corresponding Author:
La Ode Juni Akbar
junilaode23@gmail.com

DOI: 10.29303/jppipa.v11i12.13297

Abstract: This study aims to analyze the spatio-temporal dynamics of land cover for estimating the Urban Heat Island (UHI) phenomenon using Google Earth Engine (GEE) in Gorontalo City.Multi-temporal Landsat 5/7/8/9 data were processed in GEE to derive NDVI, emissivity, and Land Surface Temperature (LST). The UHI index was calculated using the statistical threshold formula UHI = Ts − (μ + 0.5σ), where values of zero or below (≤0) indicate non-UHI areas, while positive values (>0) represent areas affected by UHI. A correlation analysis was performed between field temperature, LST, and NDVI. Temporally, Gorontalo City exhibits the expansion and intensification of UHI over the 30-year period. The most evident changes are the increased area of the 0–1 and 1–2 classes enveloping the urban area, while the 2–3 class emerges as localized hotspots corresponding to areas of highest density. LST increased from 21–56 °C (1995) to 26–58 °C (2025), while NDVI declined in the city center but remained high in the southern–western zones and near water bodies. The surface temperature exhibits a strong correlation with vegetation conditions and field temperature. The main drivers of these dynamics were the increase in impervious surface fractions (asphalt/concrete) and the reduction of vegetative cover, which decreased latent heat (evapotranspiration) and increased sensible heat.

Keywords: Google Earth Engine; Normalized Difference Vegetation Index; Emissivity; Land Surface Temperature; Land Cover; Urban Heat Island

Introduction

The Urban Heat Island (UHI) phenomenon refers to the condition in which urban areas experience significantly higher temperatures compared to their surrounding rural environments. This effect arises from the accumulation of heat generated by human activities and urban development processes, such as infrastructure expansion, dense building construction, and the conversion of natural land cover into built-up areas. Numerous studies (Estoque et al., 2017; Kandel et al., 2016; Yang et al., 2016) have identified UHI as a major concern in urban climatology due to its direct impact on environmental quality, thermal comfort, and urban ecosystem sustainability. Furthermore, UHI contributes to public health challenges, including heat stress, respiratory issues, and increased energy consumption caused by the extensive use of air conditioning (Bornstein & Lin, 2000; He et al., 2007; Sekertekin et al., 2016; Tan et al., 2010).

From a physical standpoint, UHI results from modifications in the Earth's surface characteristics within urban environments, where natural elements such as vegetation and open soil are replaced by low-albedo materials like asphalt and concrete (Ming et al., 2024; Scafetta & Ouyang, 2019; Sultana & Satyanarayana, 2018). These materials have high heat absorption and retention capacities, causing surface temperatures to rise and persist, particularly at night. Large cities with high urban density tend to exhibit more intense UHI effects, as increasing building volumes and anthropogenic activities amplify localized heat accumulation (Bala et al., 2021; Liu et al., 2023; Y. Zhou et al., 2017).

This condition is also evident in Gorontalo City, which has undergone rapid urban growth over the past

How to Cite:
Akbar, L. O. J., Koto, A. G., & Rijal, A. S. (2025). Spatio-Temporal Analysis of Land Cover for Estimating UHI Using GEE in Gorontalo City. *Jurnal Penelitian Pendidikan IPA*, *11*(12), 528-540. https://doi.org/10.29303/jppipa.v11i12.13297

two decades, driven by continuous infrastructure expansion and population increase (BAPPEDA Gorontalo City, 2010). The transformation of agricultural lands and green open spaces into residential and infrastructural zones has significantly altered local land cover patterns (BPS Gorontalo City, 2021), leading to noticeable fluctuations in local surface temperature (Adiningsih et al., 2001; Duka et al., 2020; Sugini, 2014). Uncontrolled urban sprawl has further intensified the UHI phenomenon (Mirzaei, 2015; Mirzaei et al., 2012), suggesting that even if global climate conditions remain stable, urban areas will continue to experience rising local temperatures (Hassan et al., 2021).

Land cover transformation plays a crucial role in the formation of UHI, as urbanization typically reduces vegetative cover, leading to increased surface heat (Prayogi et al., 2024; Voogt & Oke, 2003; Weng et al., 2004). The loss of vegetation diminishes evapotranspiration, a natural cooling process that helps regulate temperature (Igun, 2017; Kotharkar & Bagade, 2018; Mora et al., 2017). In the central region of Gorontalo City, surface temperatures have been recorded at approximately 31–32°C, largely due to the scarcity of vegetation, heavy vehicle emissions, and the reflection of heat from asphalt and concrete surfaces (Koto, 2015)

In recent years, the use of web-based remote sensing technology, particularly through GEE, has become increasingly important for studying environmental changes. GEE's access to extensive datasets and its ability to process data quickly and efficiently have made it an essential tool in environmental research (Amani et al., 2020; Bokaie et al., 2016; Gorelick et al., 2017; Kikon et al., 2016; Tamiminia et al., 2020). It has been widely applied in studies analyzing environmental phenomena, including the Urban Heat Island (UHI) effect (Insan & Rahmi, 2024). Temporal thermal data available on the GEE platform allow for effective analysis of Land Surface Temperature (LST) trends related to UHI (Ravanelli et al., 2018).

The spatial distribution of LST can be correlated with other physical parameters, such as building density, vegetation cover, and land use patterns (Arnfield, 2003; Bornstein & Lin, 2000; Estoque et al., 2017; Liu et al., 2023; Ming et al., 2024; Y. Zhou et al., 2017). However, many previous studies using GEE have focused primarily on spatial analysis, often overlooking temporal variations that provide insights into the evolution of UHI over time.

Nonetheless, a common constraint in applying Google Earth Engine (GEE) to Urban Heat Island (UHI) studies is its predominant focus on mapping surface temperature distributions, often overlooking temporal variations. To address this limitation, the present study examines temperature changes spanning a 30-year urban development phase in Gorontalo City. Its objective is to conduct a spatio-temporal analysis of land cover to estimate UHI effects within this region using GEE.

Method

Research Location

The research was conducted in Gorontalo City, which is geographically located between 00° 28′ 17″ – 00° 35′ 56″ North Latitude and 122° 59′ 44″ – 123° 05′ 59″ East Longitude, with a total area of 64.79 km². The city is bordered by Bone Bolango Regency to the north and east, Tomini Bay to the south, and Gorontalo Regency to the west. The elevation ranges from 0 to 500 meters above sea level. The lowland areas account for approximately 60–70% of the total area (around 38.87–45.35 km²), while the hilly areas cover about 30–40% (around 19.44–25.92 km²). Gorontalo City has a tropical climate with an average temperature ranging from 23°C to 32°C and an average annual rainfall between 1,500 mm and 2,500 mm.

Tools and Materials

The tools and materials used in this research include a computer, ArcGIS software, access to GEE, GPS device, smartphone, ATM, and Landsat satellite imagery. The satellite data consist of Landsat 5 TM (May 5), Landsat 7 ETM+ (February 17), Landsat 8 OLI/TRS (October 19), and Landsat 9 (May 31), with temporal coverage for the years 1995, 2005, 2015, and 2025.

Data Acquisition Technique

Land cover identification was carried out using Landsat satellite imagery through the supervised classification method. The classification was divided into four categories: built-up land, vegetation, bare land, and water bodies. The Normalized Difference Vegetation Index (NDVI) and Land Surface Temperature (LST) data were extracted computationally from Landsat imagery using the Google Earth Engine (GEE) platform. Furthermore, field observations were conducted at several sample points to verify the accuracy of the land cover classification results.

Field Data Collection Technique

The first stage involved direct observation of the physical characteristics of Gorontalo City, including urban areas and the distribution of green open spaces. In the second stage, all observations were documented geospatially using the Global Positioning System (GPS) to record coordinates. The collected field data served as ground truth to validate the satellite image classification results. Validation was performed by comparing and matching selected sample points on the imagery with actual field conditions.

Data Analysis Technique

a) NDVI Analysis

The vegetation density map was generated using the Normalized Difference Vegetation Index (NDVI), which is calculated based on the near-infrared (NIR) and red (RED) spectral bands. NDVI values range from −1 to +1. A value close to −1 indicates bare soil or areas with sparse vegetation, while a value close to +1 represents dense vegetation. The NDVI calculation follows Equation (1) as described (Ermida et al., 2020) (Equation 1).

$$NDVI = \frac{NIR-RED}{NIR+RED} \quad (1)$$

Based on the values determined in Equation (2), the Proportion of Vegetation (PV) can be calculated, as described (Yu et al., 2014). This index is used to illustrate the extent to which a specific area is covered by vegetation compared to other surface elements, such as bare soil, water bodies, or built-up areas.

$$PV = \left[\frac{NDVI-NDVImin}{NDVImax-NDVImin}\right]^2 \quad (2)$$

b) Land Surface Temperature (LST) Analysis

The process of calculating Land Surface Temperature (LST) was conducted using Equations (3) and (4).

1) Spectral Radiance (Lλ)

Spectral radiance can be obtained from the digital number (DN) values of the TIRS band using the following equation, as described (Kafer et al., 2019).

$$L_\lambda = M_L \, x \, Q_{cal} + A \quad (3)$$

Where: Lλ represents the spectral radiance at the top of the atmosphere (TOA), expressed in units of W/(m²•sr•µm). ML is the multiplicative rescaling factor specific to each band, which can be found in the Landsat image metadata file. For the TIRS band, this factor has a value of 3.342×10^{-4} W/(m²•sr•µm). QCal denotes the digital number (DN) of the band, which ranges from 0 to 255. AL is the additive rescaling factor, also specific to the TIRS band, and is included in the image metadata file.

2) Brightness Temperature

The top-of-atmosphere (TOA) spectral radiance is converted into Brightness Temperature (T), expressed in degrees Celsius (°C), using Equation (4). The thermal conversion constants K1 and K2 for the TIRS band are provided in the metadata file accompanying the imagery. The formula used for this conversion is presented below, as described (Kafer et al., 2019; Weng et al., 2004).

$$T = \frac{K_2}{log\left(\frac{K_1}{L\lambda}+1\right)} - 273.15 \quad (4)$$

Lλ is the spectral radiance derived from Equation (3). K1 and K2 are the thermal conversion constants for the TIRS band, which are listed in the image metadata file (Landsat 5: K1 = 607.76 and K2 = 1260.56; Landsat 7: K1 = 666.09 and K2 = 1282.71; Landsat 8: K1 = 774.8853 and K2 = 1321.0789).

3) Land Surface Emissivity (ε)

The Earth's surface and its various components exhibit differences in emissivity. This factor is determined using an NDVI-based equation, as described in Equation (5) (Sharma et al., 2021).

$$\varepsilon = 0.004 \times Pv + 0.986 \quad (5)$$

4) Land Surface Temperature (LST)

By taking into account the value of Land Surface Emissivity (LSE), the Land Surface Temperature (LST) can be calculated using Equation (6), as described (Weng et al., 2004).

$$LST = \frac{T}{\left(1+\left(\lambda\frac{T}{C_2}\right)x\log(\varepsilon)\right)} \quad (6)$$

$$C^2 = \frac{h \, x \, c}{s} \quad (7)$$

Where: λ is the wavelength of the emitted radiation (for Landsat 5 and 7: λ = 11.457 µm, and for Landsat 8: λ = 10.8 µm). T is the brightness temperature derived from the Landsat data. ε represents the land surface emissivity. C_2 is the second Planck constant, with a value of 1.4388×10^{-2} m•K. h is Planck's constant, valued at 6.626×10^{-34} J•s. k is the Boltzmann constant, with a value of 1.38×10^{-23} J/K. c is the speed of light in a vacuum, with a value of 2.998×10^8 m/s.

c) Urban Heat Island (UHI)

The Urban Heat Island (UHI) value is obtained using the following equation, which is calculated based on a threshold approach. A positive value indicates the presence of a UHI effect, while a negative value (below zero) indicates its absence (Rizki et al., 2024).

$$UHI = Ts - (\mu+0{,}5\alpha) \quad (8)$$

Where: UHI: Urban Heat Island intensity (°C), Ts: Surface temperature (°C), µ: Mean land surface temperature (LST) of the study area (°C), α: Standard deviation of the LST values within the study area (°C).

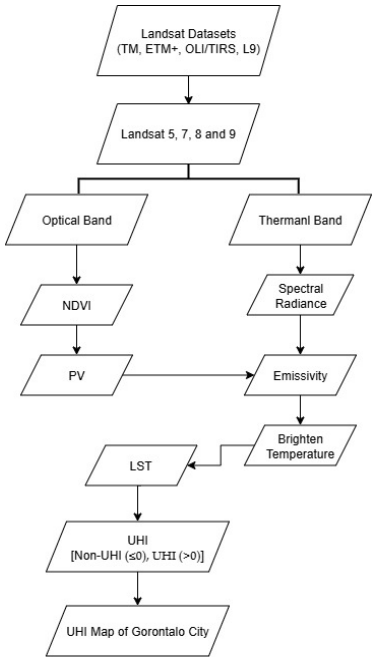

Figure 1. Research Flowchart

Result and Discussion

Overall, the 1995 baseline map provides a critical benchmark for temporal comparison, serving as a quantitative and visual reference to measure the extent, rate, and spatial direction of land cover transformations in later years (2005, 2015, and 2025). By establishing this early reference point, subsequent analyses can more accurately interpret the dynamics of urbanization, vegetation loss, and land degradation, as well as evaluate how human activity has reshaped Gorontalo City's environmental and thermal landscape over time. The 2005 map (L7 ETM+) represents a critical transition phase, capturing the expansion of built-up areas along transportation corridors and settlements, as well as the reduction of vegetation in developing zones. Due to the SLC-off issue affecting Landsat 7 imagery, gap-filling or multi-date composite processing is recommended to minimize striping bias and ensure accurate thematic mapping. After applying gap-filling corrections, NDVI values can be calculated consistently, allowing a reliable comparison of land cover changes between 1995 and 2005. The 2015 map (L8 OLI/TIRS) demonstrates significant improvements in radiometric and geometric quality, enhancing the distinction between vegetated and built-up areas. The OLI sensor provides more stable and low-noise imagery compared to previous periods, enabling more precise identification of urbanization patterns, vegetation degradation, and overall land cover dynamics.

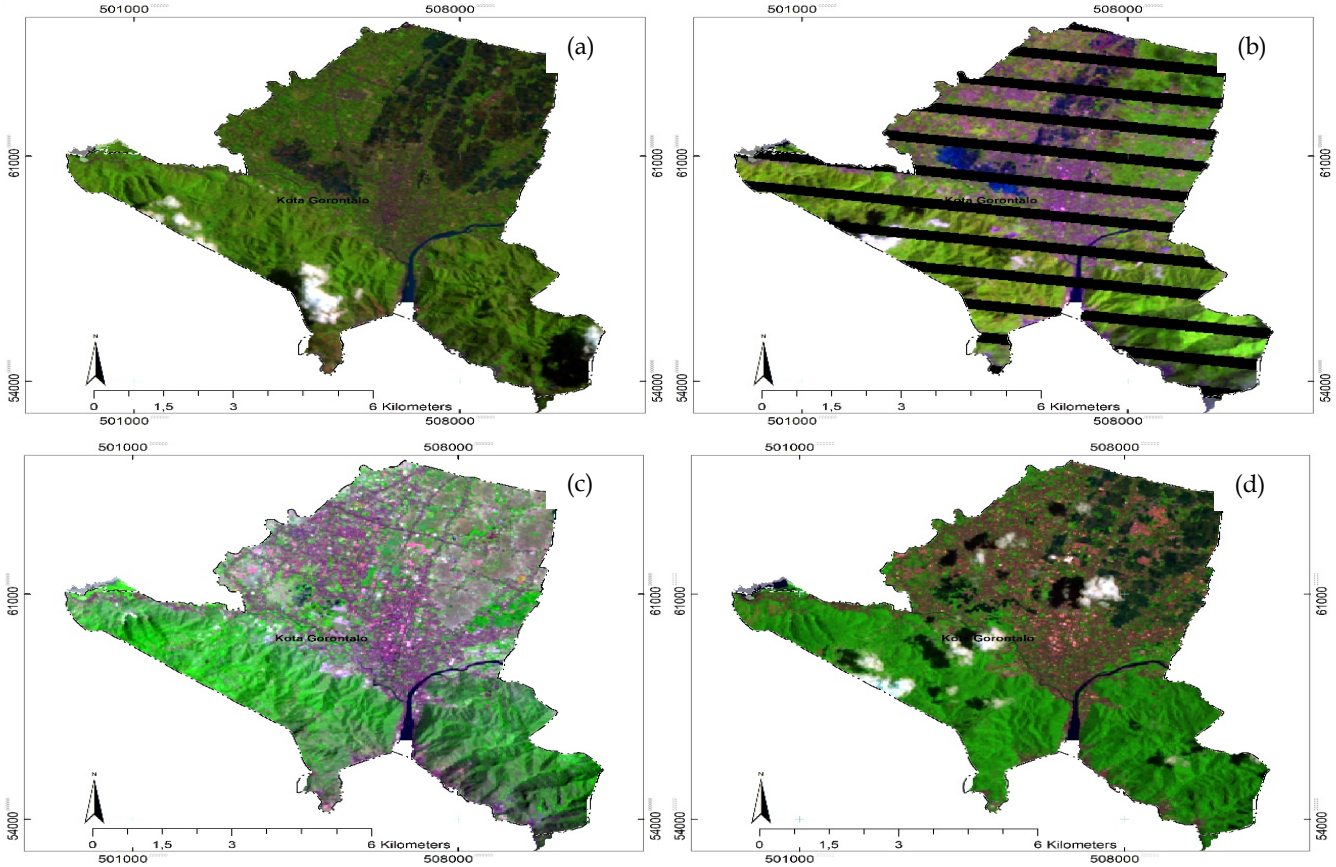

Figure 2. Landsat image of Gorontal City in 1995-2025. Landsat 5 TM May 5 (a), Landsat 7 ETM+ Feb 17 (b), Landsat 8 OLI/TRS Oct 19 (c), and Landsat 9 Mar 28 (d)

OLI-based studies in urban areas across Indonesia have shown that NDVI is an effective tool for mapping vegetation degradation associated with urban densification. It helps to clearly identify built-up expansion and changes along riverbanks and coastal zones. Cloud and shadow masking (QA/Fmask) has become a standard preprocessing step prior to classification. The 2025 map (L9 OLI-2/TIRS-2) provides spectral continuity with OLI (2015) while offering improved calibration stability (according to L9 calibration notices). Since compatibility between Landsat 8 and 9 is maintained, direct comparison of 2015–2025 land-use change trends (e.g., increasing NDBI and decreasing NDVI) can be conducted using the same preprocessing protocol.

Based on the NDVI map analysis for 1995, 2005, 2015, and 2025 in Gorontalo City, the maps represent the spatial distribution of vegetation density, classified into five value ranges. NDVI values range from –1 to +1, where the lowest class (–1 to –0.03) indicates non-vegetated surfaces such as water bodies and built-up areas. The next class (–0.03 to 0.15) represents open or barren land with minimal vegetation cover, while the intermediate classes (0.15–0.25 and 0.26–0.35) correspond to sparse to moderate vegetation, such as shrubs and grasslands. The highest class (0.36–1) signifies dense and healthy vegetation, typically found in forests and fertile plantations.

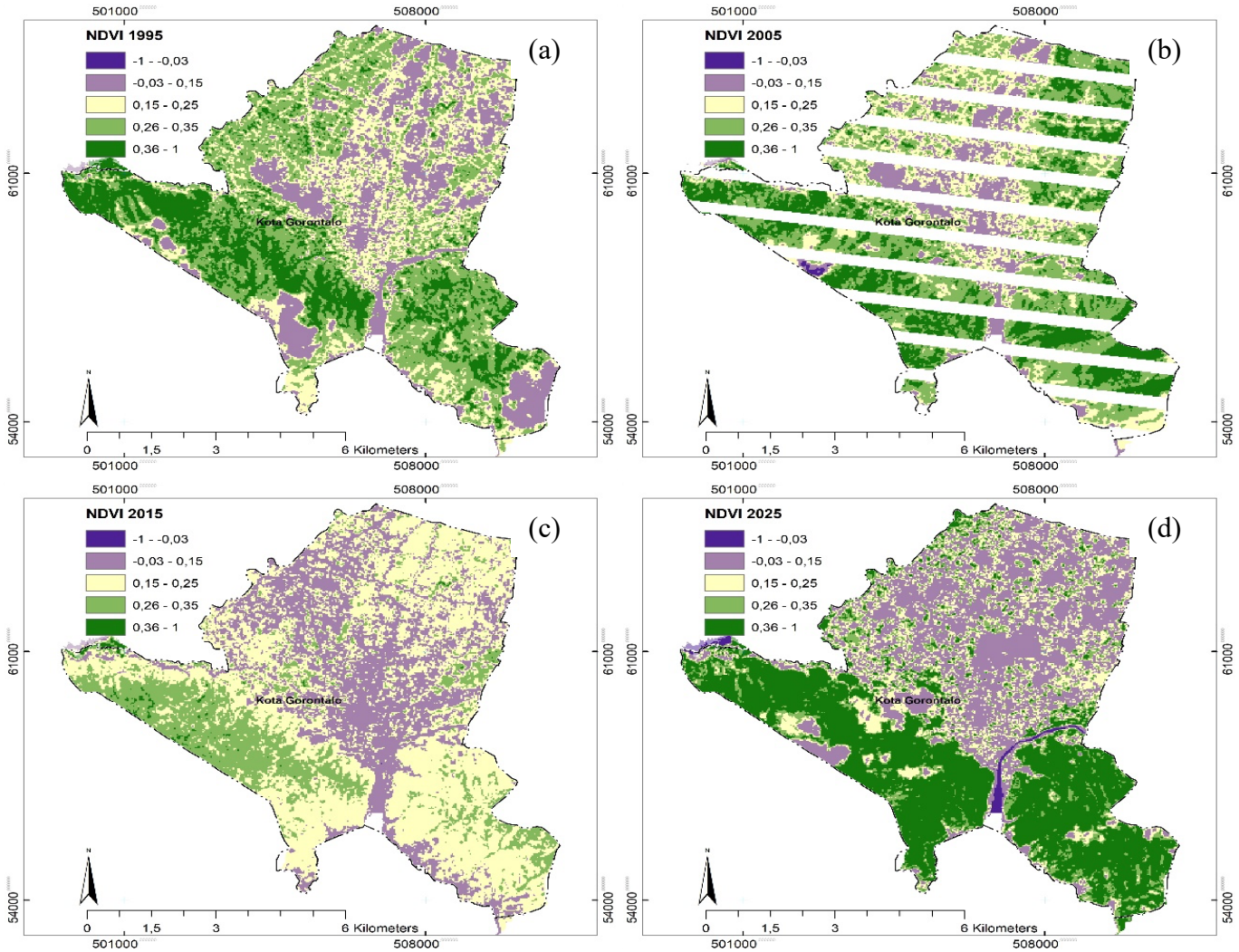

Figure 3. NDVI Classification of Goromntalo City in 1995 (a), 2005 (b), 2015 (c) and 2025 (d)

From an ecological perspective, the NDVI class distribution provides a baseline depiction of Gorontalo City's environmental condition during each period. Areas with high NDVI values play a vital role in ecosystem services, including hydrological regulation and carbon sequestration, whereas regions with low NDVI values tend to be more vulnerable to land degradation. The 1995 NDVI map, for example, shows relatively dense vegetation in the western-southern and parts of the eastern sectors (0.36–1 and 0.26–0.35 classes), indicating dense canopies and favorable moisture conditions. Conversely, low NDVI areas (–0.03–0.15) are

concentrated in the city center and development corridors, reflecting impervious surfaces, open land, or sparse vegetation. NDVI in 2005 shows that medium-to-high vegetation (≥0.26) remained dominant in the southern and western parts of Gorontalo City.

However, low DVI patches expanded noticeably in the city center and along major access corridors. Although the map contains the typical SLC-off striping artifact of Landsat 7, the spatial trends remain clearly interpretable. By 2015, NDVI values in the central area decreased further, with the –0.03–0.15 and 0.15–0.25 classes expanding, while areas with high vegetation cover became more limited. This pattern aligns with the densification of residential settlements and the conversion of green spaces, which reduced canopy coverage and evapotranspiration, thereby weakening the vegetation index (Zha et al., 2003).

By 2025, areas with high vegetation (NDVI 0.36–1) appear prominently again in the southern, western, and eastern regions, while low NDVI values continue to dominate the central and northern parts of the city. This pattern reflects the contrast between urban and non-urban landscapes, where natural and agricultural areas maintain high NDVI values, while built-up and bare lands remain within the lower NDVI range (Pettorelli et al., 2011; Huete et al., 2002). The relationship between NDVI and land surface temperature (LST) is inversely proportional, where dense vegetation acts as a natural cooling agent through the process of evapotranspiration that absorbs heat energy, while open or built-up areas tend to reflect more radiation as heat, thereby intensifying the urban heat island effect.

Based on **Figure 4**, the histogram of NDVI value distribution clearly illustrates the interannual dynamics of vegetation. In 1995, the histogram exhibits a bimodal pattern with peaks around 0.12–0.15 (representing sparse vegetation or transitional areas) and 0.32–0.36 (indicating moderately dense vegetation). This pattern reflects a mixed landscape composition between built-up zones and green areas, highlighting an early stage of urban expansion within Gorontalo City, indicating that the landscape was still a mixture of built-up areas and green zones. In 2005, the peak shifted toward a medium–high NDVI range (0.34–0.38), thus indicating that vegetation was still relatively dominant, although the tail toward lower NDVI values (water, bare soil, or built-up areas) remained present.

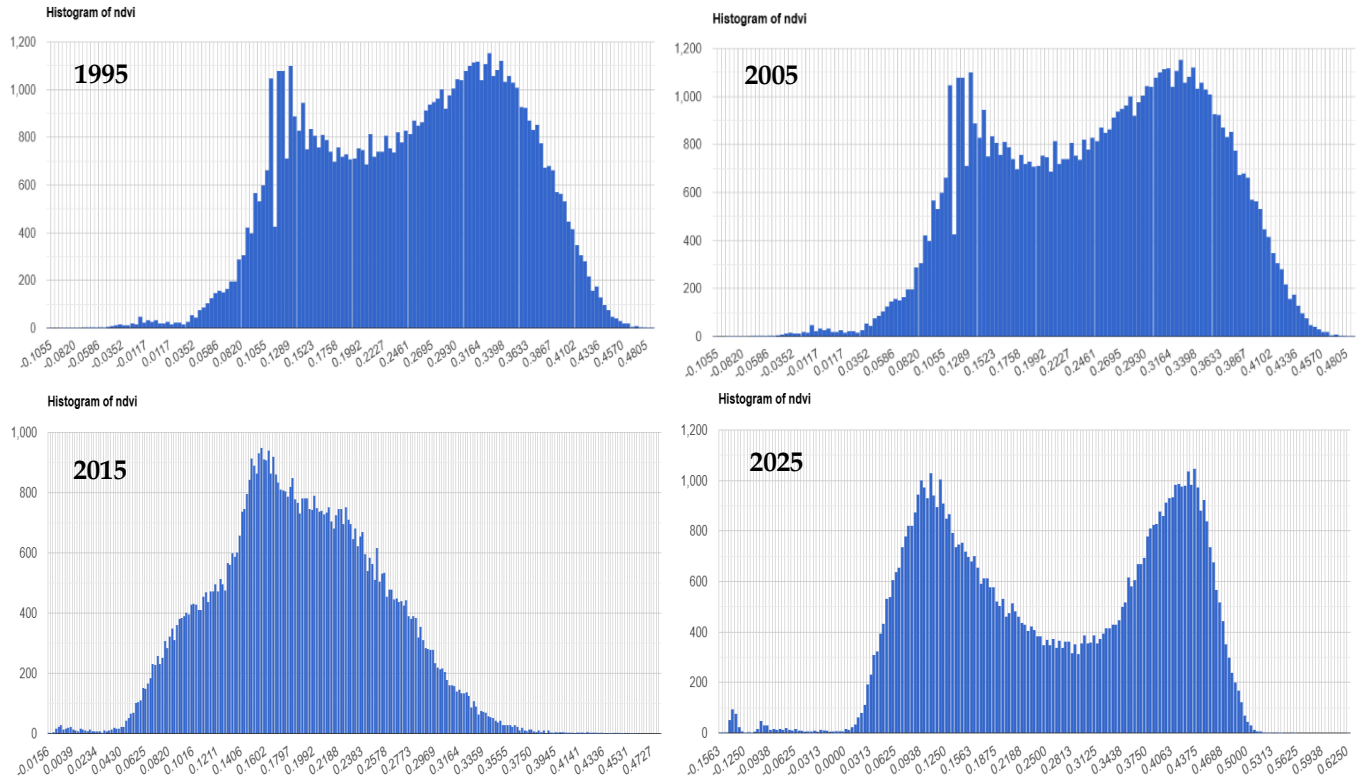

Figure 4. Histogram NDVI of Gorontalo City in 1995, 2005, 2015 and 2025

In 2015, the main mode dropped to 0.15–0.20, signifying a reduction in canopy density and an increase in non-vegetated surfaces due to intensified urban densification. By 2025, the histogram became bimodal again and more polarized, with one peak at low–medium NDVI values (0.12–0.18) representing urban cores and transitional zones, and another peak at high NDVI values (0.43–0.50) reflecting forested or densely vegetated plantation areas.

Figure 5, illustrates a negative correlation between NDVI and LST, expressed by the equation LST = −15.052•NDVI + 49.358, with R = 0.382 and R^2 = 0.146. This indicates that an increase in NDVI is associated with a decrease in surface temperature. Specifically, every 0.1-unit increase in NDVI is estimated to reduce LST by approximately 1.5 °C. This pattern aligns with biophysical theory, which states that vegetation canopies enhance evapotranspiration (transferring energy into latent heat), provide shading, and generally exhibit high emissivity—thereby reducing the amount of sensible heat that is emitted back and detected by thermal sensors.

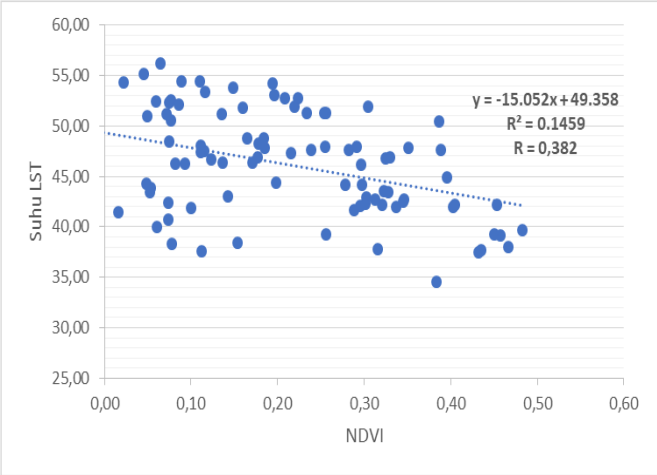

Figure 5. Correlation Graph between LST and NDVI

Conversely, areas with low NDVI values—typically impervious surfaces such as asphalt and concrete—tend to have relatively low albedo, limited water retention capacity, and restricted ventilation. As a result, these areas exhibit higher LST values, contributing to the formation of urban heat islands (UHI) (Peng et al., 2012; Weng, 2009; D. Zhou et al., 2014).

Figure 6. The 1995 LST analysis shows that surface temperatures ranged between 21–56°C. Lower temperatures (21–30°C) were mostly found in forested areas and water bodies, particularly in the southern and western parts of the city. In contrast, higher temperatures (43–56°C) were dominant in the downtown area of Gorontalo and its surroundings, indicating a concentration of residential settlements and extensive impervious surfaces. These findings suggest that even in the early stage of urbanization, the UHI effect had already begun to emerge in the city center. This aligns with the concept of UHI, which states that urban centers tend to be warmer due to the dominance of impervious surfaces and limited vegetation cover (Voogt & Oke, 2003).

In 2005, the LST distribution ranged from 6–49°C. The map indicates an expansion of areas within the medium to high-temperature classes (29–34°C and 34–49°C), extending toward the suburban regions. Lower temperatures (6–19°C) were mainly observed in densely vegetated areas and water bodies. Although there were data stripes caused by the SLC-off issue in Landsat 7, the general trend still shows increasing temperatures in urban areas (Sobrino et al., 2004). Subsequently, the 2015 LST results show a temperature range of 29–50°C. High-temperature zones (42–50°C) became increasingly dominant in the northern and central parts of the city, especially in densely populated residential areas. Meanwhile, low-temperature zones (29–35°C) remained only in heavily vegetated regions in the south and along river corridors. This indicates a stronger impact of urbanization and a significant reduction in vegetation cover, which lessens the ability to mitigate temperature increases (Weng et al., 2004)

By 2025, LST values are projected to range between 26–58°C. High temperatures (49–58°C) are widespread across the city center and expanding urban areas, while low temperatures (26–35°C) persist mainly in dense vegetation zones and water bodies. This confirms the intensification of the UHI phenomenon, with a more pronounced thermal contrast distinguishing urban from non-urban areas (Y. Zhou et al., 2017).

Changes in LST during the 1995–2005 period indicate an increase in surface temperature within urban zones, driven by residential expansion, infrastructure development, and vegetation loss in the city core. From 2005 to 2015, high-temperature areas continued to expand, particularly in downtown regions, due to population growth and the conversion of green spaces into built-up areas. These changes are consistent with the trend of increasing UHI in developing cities. Then, in the period of 2015–2025, the temperature surge was more significant, with the maximum value reaching 58°C.

The main causes are massive urbanization, dense building concentration, the reduction of green open spaces, and the increase in vehicular activity that contributes to anthropogenic heat emissions. Vegetated areas and water bodies exhibit lower LST values due to the cooling effects of evapotranspiration and the high heat capacity of water, whereas concrete and asphalt surfaces absorb and retain heat for longer periods, resulting in higher LST. This phenomenon is consistent with global findings showing that large cities tend to experience higher LST compared to their surrounding areas (Peng et al., 2012).

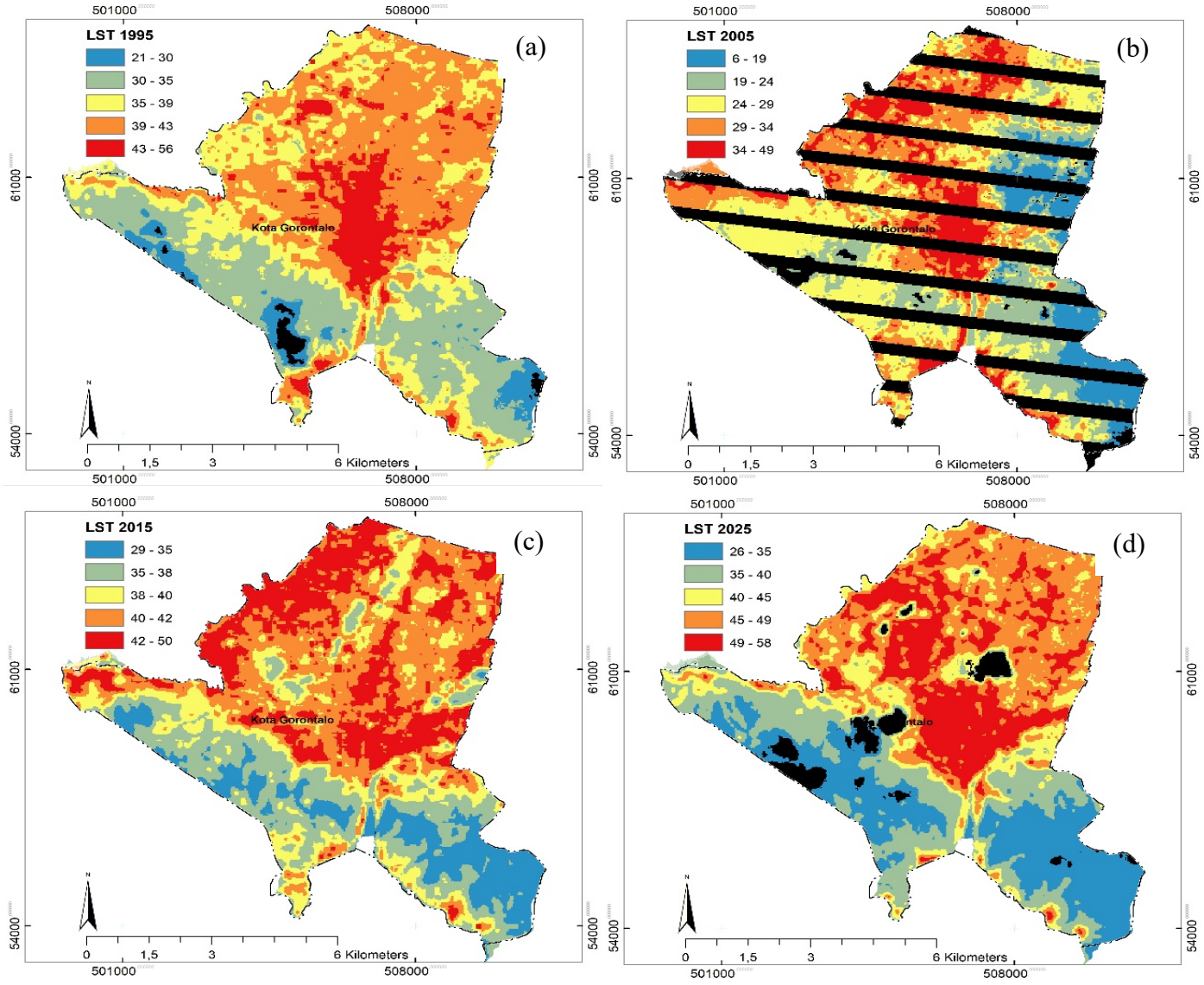

Figure 6. LST of Goromntalo City in 1995 (a), 2005 (b), 2015 (c) and 2025 (d)

Spatial analysis of LST over the 30-year period (1995–2025) indicates a significant increase in surface temperature alongside the growth of Gorontalo City. The most substantial change occurred during the 2015–2025 period, highlighting the acceleration of urbanization and the decline of natural vegetation cover. This phenomenon supports the theory that the conversion of vegetated land into built-up areas is the primary factor driving the increase in LST within urban environments. The increase in LST in urban areas highlights the need for spatial planning that emphasizes a balance between infrastructure development and the provision of green open spaces (Insan & Rahmi, 2024).

Figure 7, shows a positive correlation between air temperature measured in the field (x) and LST (y), represented by the linear model y = 0.4132x + 14.664. The correlation coefficient (R) of 0.693 indicates a strong relationship, while the coefficient of determination (R^2 = 0.480) suggests that approximately 48% of the variation in LST can be explained by variations in air temperature. In other words, nearly half of the changes in LST move in the same direction as changes in observed air temperature, while the remainder is influenced by other factors. The regression slope of 0.413 means that for every 1°C increase in air temperature, the average LST rises by approximately 0.41°C. A regression slope of <1 is physically reasonable, as LST and air temperature measured at an altitude of around 1.5–2 meters are not identical quantities and respond differently to surface energy balance processes.

It is physically acceptable because LST and air temperature measured at a height of approximately 1.5–2 meters are not identical quantities and respond differently to the surface energy balance. The differences between them are influenced by several factors: (1) the difference in observation scale — LST represents

the average value of a pixel of about 30 meters, while field temperature is a point-based measurement; (2) the temporal mismatch between the satellite overpass time and the field measurement time; (3) variations in surface emissivity and material types; and (4) the influence of urban morphology and soil moisture.

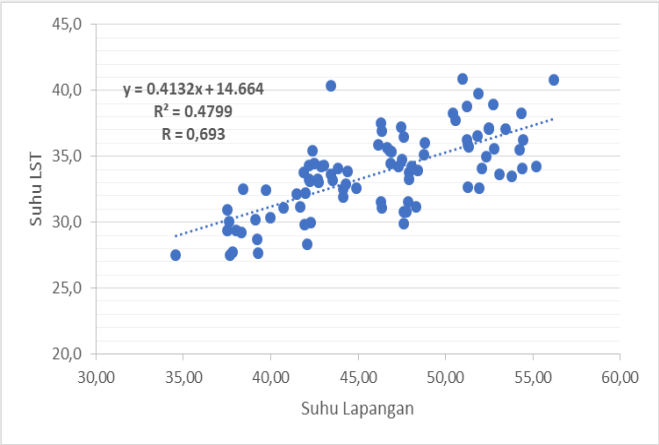

Figure 7. Correlation Graph Between LST and Field Temperatur

Figure 8. Based on the analysis results, areas with zero or negative values (≤0) indicate regions unaffected by the Urban Heat Island (UHI) phenomenon, while positive values (>0) represent areas experiencing UHI. The affected regions were further classified according to the intensity of their UHI values. In 1995, UHI was concentrated in the central part of Gorontalo City with moderate to high intensity, while forested and water-covered areas remained relatively cool. By 2005, UHI zones expanded along road corridors and newly developed residential areas. Despite data gaps caused by SLC-off issues, the core–periphery pattern remained evident. In 2015, more UHI clusters appeared in densely built-up zones, whereas vegetated and aquatic areas maintained cooler conditions. By 2025, UHI intensity had become significantly stronger in the city center, while dense vegetation cover and water bodies functioned as local thermal buffers.

These findings reveal the progressive development of UHI in line with the increasing extent and density of built-up land (Hassan et al., 2021; Mohajerani et al., 2017; Voogt & Oke, 2003; Weng, 2009). The 1995–2005 period was characterized by UHI expansion driven by the conversion of green land into residential and infrastructure areas. The 2005–2015 period demonstrated UHI consolidation into distinct heat clusters following building densification, reduced surface albedo, and limited urban ventilation. Finally, the 2015–2025 period experienced UHI intensification, triggered by rising anthropogenic heat emissions (from vehicles and air conditioning), fragmentation of green open spaces, and an increase in impervious surface fractions, which reduced evapotranspiration (Imhoff et al., 2010; Peng et al., 2012; D. Zhou et al., 2014).

Non-UHI areas (<0) were observed in regions with dense vegetation and water bodies, where evapotranspiration and the high heat capacity of water helped lower surface temperatures. Moderate UHI zones (0–1 to 1–2) were typically found in transitional areas—moderately dense residential zones and open lands—where the combination of built materials and vegetation created a warmer but still balanced surface energy state. High UHI intensity (2–3) appeared in the city center and densely populated residential areas, dominated by asphalt and concrete (low albedo, high thermal inertia), low surface moisture, and strong anthropogenic heat. These conditions redirected energy into sensible heat, resulting in higher and longer-lasting surface temperatures (Ullah et al., 2023; Voogt & Oke, 2003). Between 1995 and 2005, UHI zones (1–2) expanded outward from the city core toward suburban areas, driven by the conversion of vegetated land into built-up zones and improved road connectivity. From an energy balance perspective, the growing fraction of impervious surfaces reduced latent heat (due to less evapotranspiration) while increasing sensible heat (Oke, T. R., 1982; Weng, 2009).

During 2005–2015, the UHI pattern transformed from a single hotspot into multiple clustered heat zones following urban densification. The influence of urban morphology and low-albedo materials became more dominant, while fragmented vegetation was no longer sufficient to balance daytime peak heat (Voogt & Oke, 2003; D. Zhou et al., 2014). By 2015–2025, the intensity further increased, with the spatial extent of classes 0–1 and 1–2 expanding, and localized 2–3 hotspots persisting or emerging. Besides surface properties, anthropogenic heat from vehicles, small industries, and air conditioning systems also contributed to excess energy, particularly during nighttime. Green zones and water bodies remained effective in mitigating local UHI effects; however, the fragmentation of green spaces reduced the overall cooling effect at the city scale (Hassan et al., 2021; Imhoff et al., 2010; Li et al., 2020). Temporally, Gorontalo City exhibited both expansion and intensification of UHI from 1995 to 2025. The most evident changes included the broadening of classes 0–1 and 1–2, which covered most urban areas, while class 2–3 hotspots became localized around the highest-density pockets. This trend aligns with global findings indicating that the proportion of impervious surfaces and vegetation cover are the two main controlling factors, further influenced by urban morphology and anthropogenic heat generation (Chatterjee & Majumdar, 2022).

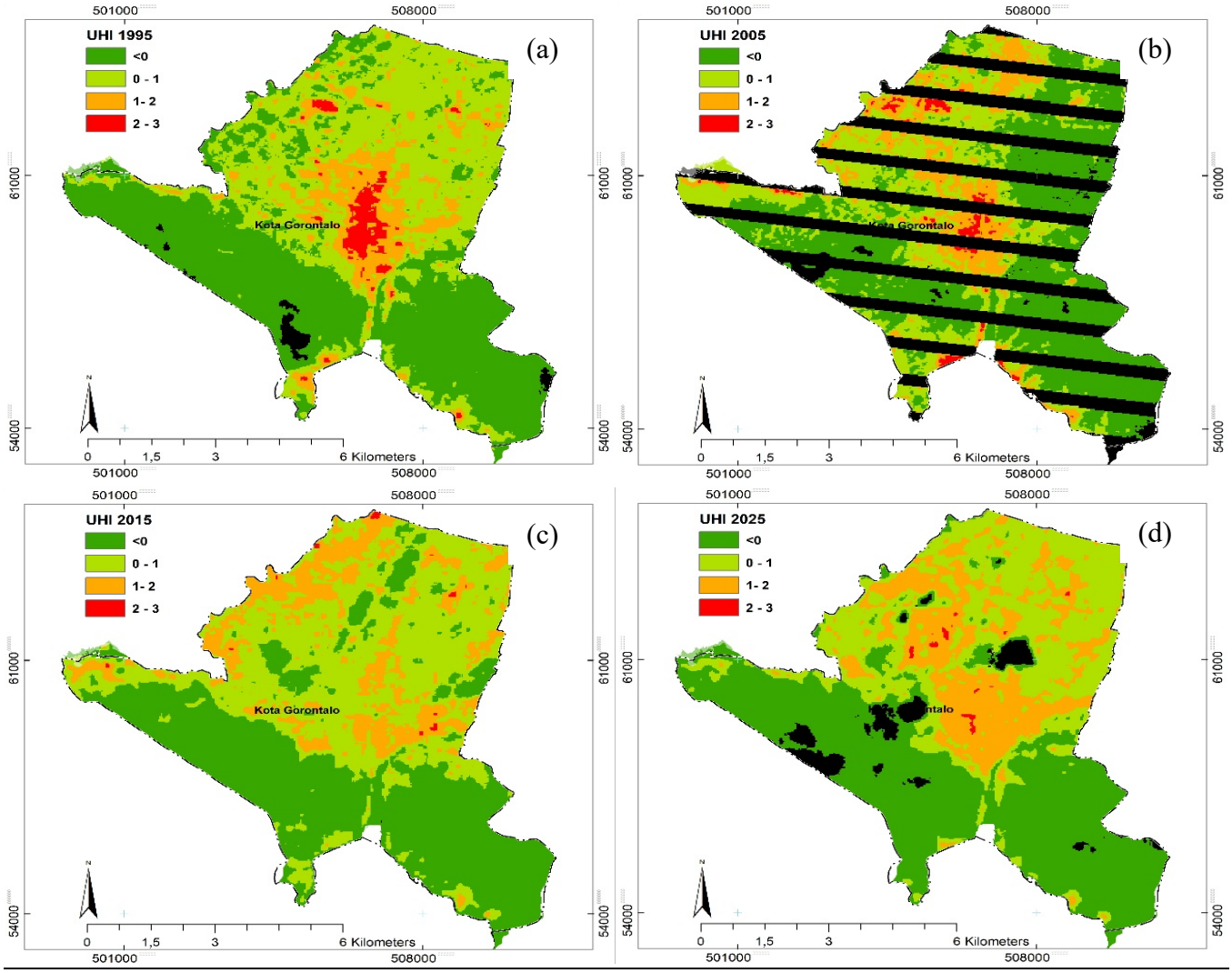

Figure 8. UHI of Goromntalo City in 1995 (a), 2005 (b), 2015 (c) and 2025 (d)

Conclusion

The UHI analysis revealed that pixels with values ≤0 represented non-UHI zones, while those >0 indicated UHI-affected areas with varying intensity. From 1995 to 2025, Gorontalo City experienced continuous UHI expansion and intensification—from initial concentration in the city center (1995), spreading along transportation corridors and new residential areas (2005), forming clustered heat zones in dense built-up areas (2015), to intensification in 2025 with localized hotspots in the most crowded regions. In contrast, densely vegetated and aquatic areas consistently acted as thermal buffers. The main driving forces behind these dynamics include the increasing proportion of impervious surfaces (asphalt/concrete) and decreasing vegetation cover, which collectively reduce latent heat (evapotranspiration) while increasing sensible heat. Additional contributing factors include urban morphology (building density and height ratio that restrict airflow), low surface albedo, and anthropogenic heat from transportation, air conditioning, and commercial activity. These combined factors explain the dominance of moderate UHI classes (0–1 and 1–2) across urban areas and the emergence of localized hotspots (2–3) in the densest sectors of the city.

Acknowledgments

The authors express their sincere gratitude to their supervisors, Arthur Gani Koto and Ahmad Syamsu Rijal, for their scientific guidance, methodological direction, and constructive feedback throughout the research process, as well as their technical assistance during the preparation of this paper. The authors also thank the Geography Study Program, Universitas Muhammadiyah Gorontalo, for the support and permission provided during the research.

Author Contributions

LO.JA was responsible for conceptualization and problem formulation, methodological design, drafting, reviewing, editing, and thematic map preparation. AGK contributed to analytical design (LST, UHI, NDVI), data processing, and visualization. ASR provided methodological guidance,

scientific supervision, substantive feedback, and approval of the final manuscript.

Funding
This research did not receive any specific grant from public, commercial, or institutional funding agencies. All fieldwork, computational, and publication costs were fully covered by the authors.

Conflicts of Interest
The authors declare that there are no conflicts of interest.

References

Adiningsih, E. S., Soenarmo, S. H., & Mujiasih, S. (2001). Kajian Perubahan Distribusi Spasial Suhu Udara Akibat. *Jurnal Lapan*, *February*, 29–44. https://www.researchgate.net/publication/271966779_kajian_perubahan_distribusi_spasial_suhu_udara_akibat_perubahan_penutup_lahan_Studi_Kasus_Cekungan_Bandung

Amani, M., Ghorbanian, A., Ahmadi, S. A., Kakooei, M., Moghimi, A., Mirmazloumi, S. M., Moghaddam, S. H. A., Mahdavi, S., Ghahremanloo, M., Parsian, S., Wu, Q., & Brisco, B. (2020). Google Earth Engine Cloud Computing Platform for Remote Sensing Big Data Applications: A Comprehensive Review. *IEEE Journal of Selected Topics in Applied Earth Observations and Remote Sensing*, *13*(September), 5326–5350. https://doi.org/10.1109/JSTARS.2020.3021052

Arnfield, A. J. (2003). Two decades of urban climate research: A review of turbulence, exchanges of energy and water, and the urban heat island. *International Journal of Climatology*, *23*(1), 1–26. https://doi.org/10.1002/joc.859

Bala, R., Prasad, R., & Yadav, V. P. (2021). Quantification of urban heat intensity with land use/land cover changes using Landsat satellite data over urban landscapes. *Theoretical and Applied Climatology*, *145*(1–2). https://doi.org/10.1007/s00704-021-03610-3

Bokaie, M., Zarkesh, M. K., Arasteh, P. D., & Hosseini, A. (2016). Assessment of Urban Heat Island based on the relationship between land surface temperature and Land Use/ Land Cover in Tehran. *Sustainable Cities and Society*, *23*, 94–104. https://doi.org/10.1016/j.scs.2016.03.009

Bornstein, R., & Lin, Q. (2000). Urban heat islands and summertime convective thunderstorms in Atlanta: Three case studies. *Atmospheric Environment*, *34*(3), 507–516. https://doi.org/10.1016/S1352-2310(99)00374-X

Chatterjee, U., & Majumdar, S. (2022). Impact of land use change and rapid urbanization on urban heat island in Kolkata city : A remote sensing based perspective. *Journal of Urban Management*, *11*(1), 59–71. https://doi.org/10.1016/j.jum.2021.09.002

Duka, M., Lihawa, F., & Rahim, S. (2020). Perubahan Tutupan Lahan dan Pengaruhnya Terhadap Pola Persebaran Suhu di Kota Gorontalo. *Jambura Geoscience Review*, *2*(1), 16–29. https://doi.org/10.34312/jgeosrev.v2i1.2682

Ermida, S. L., Soares, P., Mantas, V., Göttsche, F. M., & Trigo, I. F. (2020). Google earth engine open-source code for land surface temperature estimation from the landsat series. *Remote Sensing*, *12*(9), 1–21. https://doi.org/10.3390/RS12091471

Estoque, R. C., Murayama, Y., & Myint, S. W. (2017). Effects of landscape composition and pattern on land surface temperature: An urban heat island study in the megacities of Southeast Asia. *Science of the Total Environment*, *577*, 349–359. https://doi.org/10.1016/j.scitotenv.2016.10.195

Gorelick, N., Hancher, M., Dixon, M., Ilyushchenko, S., Thau, D., & Moore, R. (2017). Google Earth Engine: Planetary-scale geospatial analysis for everyone. *Remote Sensing of Environment*, *202*, 18–27. https://doi.org/10.1016/j.rse.2017.06.031

Hassan, T., Zhang, J., Prodhan, F. A., Pangali Sharma, T. P., & Bashir, B. (2021). Surface urban heat islands dynamics in response to lulc and vegetation across south asia (2000–2019). *Remote Sensing*, *13*(16), 1–24. https://doi.org/10.3390/rs13163177

He, J. F., Liu, J. Y., Zhuang, D. F., Zhang, W., & Liu, M. L. (2007). Assessing the effect of land use/land cover change on the change of urban heat island intensity. *Theoretical and Applied Climatology*, *90*(3–4), 217–226. https://doi.org/10.1007/s00704-006-0273-1

Igun, E. (2017). Analysis and Sustainable Management of Urban Growth's Impact on Land Surface Temperature in Lagos, Nigeria. *Journal of Remote Sensing & GIS*, *06*(04). https://doi.org/10.4172/2469-4134.1000212

Imhoff, M. L., Zhang, P., Wolfe, R. E., & Bounoua, L. (2010). Remote sensing of the urban heat island effect across biomes in the continental USA. *Remote Sensing of Environment*, *114*(3), 504–513. https://doi.org/10.1016/j.rse.2009.10.008

Insan, K., & Rahmi, N. (2024). *The use of Landsat-8 in Google Earth Engine to analyze Urban The use of Landsat-8 in Google Earth Engine to analyze Urban Heat Island in Bogor City*. *29*(2). https://doi.org/10.17977/um017v29i22024p121-134

Kafer, P. S., Rolim, S. B. A., Iglesias, M. L., Da Rocha, N. S., & Diaz, L. R. (2019). Land surface temperature retrieval by landsat 8 thermal band: Applications of laboratory and field measurements. *IEEE Journal of Selected Topics in Applied Earth Observations and Remote Sensing*, *12*(7), 2332–2341. https://doi.org/10.1109/JSTARS.2019.2913822

Kandel, H., Melesse, A., & Whitman, D. (2016). An

analysis on the urban heat island effect using radiosonde profiles and Landsat imagery with ground meteorological data in South Florida. *International Journal of Remote Sensing*, *37*(10), 2313–2337. https://doi.org/10.1080/01431161.2016.1176270

Kikon, N., Singh, P., Singh, S. K., & Vyas, A. (2016). Assessment of urban heat islands (UHI) of Noida City, India using multi-temporal satellite data. *Sustainable Cities and Society*, *22*, 19–28. https://doi.org/10.1016/j.scs.2016.01.005

Kotharkar, R., & Bagade, A. (2018). Local Climate Zone classification for Indian cities: A case study of Nagpur. *Urban Climate*, *24*, 369–392. https://doi.org/10.1016/j.uclim.2017.03.003

Koto, A. G. (2015). Analisis suhu permukaan Kota Gorontalo dan sekitarnya menggunakan saluran thermal Citra Landsat 7 ETM +. *Prosiding Seminar Nasional Penginderaan Jauh*, *4*(1), 336–343.

Li, L., Zha, Y., & Zhang, J. (2020). Spatially non-stationary effect of underlying driving factors on surface urban heat islands in global major cities. *International Journal of Applied Earth Observation and Geoinformation*, *90*(August 2019), 102131. https://doi.org/10.1016/j.jag.2020.102131

Liu, B., Guo, X., & Jiang, J. (2023). How Urban Morphology Relates to the Urban Heat Island Effect: A Multi-Indicator Study. *Sustainability (Switzerland)*, *15*(14). https://doi.org/10.3390/su151410787

Ming, T., Liu, Y., Shi, T., Peng, C., Chen, Y., de Richter, R., & Fang, Y. (2024). Numerical investigation of urban heat island effect in various urban forms. *Energy and Built Environment*, *February*. https://doi.org/10.1016/j.enbenv.2024.11.001

Mirzaei, P. A. (2015). Recent challenges in modeling of urban heat island. *Sustainable Cities and Society*, *19*, 200–206. https://doi.org/10.1016/j.scs.2015.04.001

Mirzaei, P. A., Haghighat, F., Nakhaie, A. A., Yagouti, A., Giguère, M., Keusseyan, R., & Coman, A. (2012). Indoor thermal condition in urban heat Island - Development of a predictive tool. *Building and Environment*, *57*, 7–17. https://doi.org/10.1016/j.buildenv.2012.03.018

Mohajerani, A., Bakaric, J., & Jeffrey-Bailey, T. (2017). The urban heat island effect, its causes, and mitigation, with reference to the thermal properties of asphalt concrete. *Journal of Environmental Management*, *197*(January), 522–538. https://doi.org/10.1016/j.jenvman.2017.03.095

Mora, C., Dousset, B., Caldwell, I. R., Powell, F. E., Geronimo, R. C., Bielecki, C. R., Counsell, C. W. W., Dietrich, B. S., Johnston, E. T., Louis, L. V., Lucas, M. P., Mckenzie, M. M., Shea, A. G., Tseng, H., Giambelluca, T. W., Leon, L. R., Hawkins, E., & Trauernicht, C. (2017). Global risk of deadly heat. *Nature Climate Change*, *7*(7), 501–506. https://doi.org/10.1038/nclimate3322

Oke, T. R. (1982). The energetic basis of the urban heat island," Quarterly Journal of the Royal Meteorological Society. In *Journal of Royal Meteorological Society* (Vol. 108, pp. 1–24).

Peng, S., Piao, S., Ciais, P., Friedlingstein, P., Ottle, C., Bréon, F. M., Nan, H., Zhou, L., & Myneni, R. B. (2012). Surface urban heat island across 419 global big cities. *Environmental Science and Technology*, *46*(2), 696–703. https://doi.org/10.1021/es2030438

Prayogi, H., Setiadi, H., Supriatna, S., & Dewayany, D. (2024). Land cover change analysis in Majalengka Regency using the pan-sharpening method and random forest machine learning algorithm. *Jurnal Pendidikan Geografi: Kajian, Teori, Dan Praktek Dalam Bidang Pendidikan Dan Ilmu Geografi*, *28*(2), 178–192. https://doi.org/10.17977/um017v28i22023p178-192

Ravanelli, R., Nascetti, A., Cirigliano, R. V., Di Rico, C., Leuzzi, G., Monti, P., & Crespi, M. (2018). Monitoring the impact of land cover change on surface urban heat island through Google Earth Engine: Proposal of a global methodology, first applications and problems. *Remote Sensing*, *10*(9), 1–21. https://doi.org/10.3390/rs10091488

Scafetta, N., & Ouyang, S. (2019). Detection of UHI bias in China climate network using Tmin and Tmax surface temperature divergence. *Global and Planetary Change*, *181*(July), 102989. https://doi.org/10.1016/j.gloplacha.2019.102989

Sekertekin, A., Kutoglu, S. H., & Kaya, S. (2016). Evaluation of spatio-temporal variability in Land Surface Temperature: A case study of Zonguldak, Turkey. *Environmental Monitoring and Assessment*, *188*(1), 1–15. https://doi.org/10.1007/s10661-015-5032-2

Sharma, R., Pradhan, L., Kumari, M., & Bhattacharya, P. (2021). Assessing urban heat islands and thermal comfort in Noida City using geospatial technology. *Urban Climate*, *35*(October 2020), 100751. https://doi.org/10.1016/j.uclim.2020.100751

Sobrino, J. A., Jiménez-Muñoz, J. C., & Paolini, L. (2004). Land surface temperature retrieval from LANDSAT TM 5. *Remote Sensing of Environment*, *90*(4), 434–440. https://doi.org/10.1016/j.rse.2004.02.003

Sugini. (2014). *Kenyamanan Termal Ruang (Konsep dan Penerapan pada Desain)* (p. 251). https://fcep.uii.ac.id/karya-ilmiah/SUGINI/Buku - Kenyamanan Termal Ruang Konsep dan Penerapan pada Desain.pdf

Sultana, S., & Satyanarayana, A. N. V. (2018). Urban heat island intensity during winter over metropolitan cities of India using remote-sensing techniques: impact of urbanization. *International Journal of*

Remote Sensing, *39*(20), 6692–6730. https://doi.org/10.1080/01431161.2018.1466072

Tamiminia, H., Salehi, B., Mahdianpari, M., Quackenbush, L., Adeli, S., & Brisco, B. (2020). Google Earth Engine for geo-big data applications: A meta-analysis and systematic review. *ISPRS Journal of Photogrammetry and Remote Sensing*, *164*(May), 152–170. https://doi.org/10.1016/j.isprsjprs.2020.04.001

Tan, J., Zheng, Y., Tang, X., Guo, C., Li, L., Song, G., Zhen, X., Yuan, D., Kalkstein, A. J., Li, F., & Chen, H. (2010). The urban heat island and its impact on heat waves and human health in Shanghai. *International Journal of Biometeorology*, *54*(1), 75–84. https://doi.org/10.1007/s00484-009-0256-x

Ullah, N., Siddique, M. A., Ding, M., Grigoryan, S., Khan, I. A., Kang, Z., Tsou, S., Zhang, T., Hu, Y., & Zhang, Y. (2023). The Impact of Urbanization on Urban Heat Island: Predictive Approach Using Google Earth Engine and CA-Markov Modelling (2005–2050) of Tianjin City, China. *International Journal of Environmental Research and Public Health*, *20*(3). https://doi.org/10.3390/ijerph20032642

Voogt, J. A., & Oke, T. R. (2003). Thermal remote sensing of urban climates. *Remote Sensing of Environment*, *86*(3), 370–384. https://doi.org/10.1016/S0034-4257(03)00079-8

Weng, Q. (2009). Thermal infrared remote sensing for urban climate and environmental studies: Methods, applications, and trends. *ISPRS Journal of Photogrammetry and Remote Sensing*, *64*(4), 335–344. https://doi.org/10.1016/j.isprsjprs.2009.03.007

Weng, Q., Lu, D., & Schubring, J. (2004). Estimation of land surface temperature-vegetation abundance relationship for urban heat island studies. *Remote Sensing of Environment*, *89*(4), 467–483. https://doi.org/10.1016/j.rse.2003.11.005

Yang, L., Qian, F., Song, D. X., & Zheng, K. J. (2016). Research on Urban Heat-Island Effect. *Procedia Engineering*, *169*, 11–18. https://doi.org/10.1016/j.proeng.2016.10.002

Yu, X., Guo, X., & Wu, Z. (2014). Land surface temperature retrieval from landsat 8 TIRS-comparison between radiative transfer equation-based method, split window algorithm and single channel method. *Remote Sensing*, *6*(10), 9829–9852. https://doi.org/10.3390/rs6109829

Zha, Y., Gao, J., & Ni, S. (2003). Use of normalized difference built-up index in automatically mapping urban areas from TM imagery. *International Journal of Remote Sensing*, *24*(3), 583–594. https://doi.org/10.1080/01431160304987

Zhou, D., Zhao, S., Liu, S., Zhang, L., & Zhu, C. (2014). Surface urban heat island in China's 32 major cities: Spatial patterns and drivers. *Remote Sensing of Environment*, *152*, 51–61. https://doi.org/10.1016/j.rse.2014.05.017

Zhou, Y., Zhuang, Z., Yang, F., Yu, Y., & Xie, X. (2017). Urban morphology on heat island and building energy consumption. *Procedia Engineering*, *205*, 2401–2406. https://doi.org/10.1016/j.proeng.2017.09.862